Int. J. Heat Mass Transfer. Vol. 36, No. 13, pp. 3311–3328, 1993
Printed in Great Britain

0017–9310/93 $6.00+0.00

Unsteady flow and heat transfer for cylinder pairs in a channel

K. TATSUTANI, R. DEVARAKONDA and J. A. C. HUMPHREY†

Computer Mechanics Laboratory, Department of Mechanical Engineering, University of California at Berkeley, Berkeley, CA 94720, U.S.A.

(*Received* 27 *July* 1992 *and in final form* 25 *November* 1992)

Abstract—The incompressible, two-dimensional, unsteady flow past a pair of cylinders of square cross-section, placed in tandem normal to the flow in a channel, has been investigated by dye visualization and direct numerical simulation. The objective has been to evaluate the effect of cylinder separation distance, λ, on the flow behavior and heat transfer, for cylinder diameter ratios, D/d, of 1 and 2 over a range of Reynolds numbers $200 \leqslant Re \leqslant 1600$, based on the larger (downstream) cylinder diameter. A comparison between the experimental and numerical results for cylinders of equal cross-section dimensions shows very good agreement. The results for $D/d = 1$ reveal three distinct flow patterns as a function of λ and Re which, apparently, have not been previously reported: (1) For $0.25 \leqslant \lambda \leqslant 4$ with $Re \leqslant 200$, the inter-cylinder flow consists of a pair of steady counter-rotating eddies which do not exchange fluid with the surrounding flow and eddy shedding is observed only for the downstream cylinder. (2) For $0.25 \leqslant \lambda \leqslant 1.0$ with $400 \leqslant Re \leqslant 1600$, vertical flow oscillations arise in the inter-cylinder space, and the periodic ingestion of backward-jetting fluid from the top and bottom walls of the downstream cylinder into the inter-cylinder space is observed. For fixed λ the unsteadiness increases with Re but only the downstream cylinder sheds large eddies. (3) At a critical inter-cylinder spacing related to Re according to $\lambda_c \sim Re^{-2/3}$, the shedding of large eddies also occurs at the upstream cylinder and this results in a highly mixed inter-cylinder flow. For a cylinder diameter ratio of $D/d = 2$, with the smaller cylinder located upstream of the larger heated cylinder, it is shown that for Re fixed an optimal location exists for the upstream cylinder such that the heat transfer from the downstream cylinder is maximized. The optimal location corresponds to a spacing smaller than the critical inter-cylinder spacing.

1. INTRODUCTION

THE RELIABILITY of electronic systems, especially in computer equipment, is largely dependent on maintaining the temperatures of system components below a critical operating point. As component densities have increased with advances in packaging and circuit integration, so have the power dissipation requirements of the systems. Thus, thermal considerations have become increasingly important in the packaging of electronic components.

To address the issue of component cooling, the use of an 'eddy promoter' is suggested to alter the flow around a hot object and thereby increase the heat transfer from that object. Although some additional space may be required to place an eddy promoter in the vicinity of the object to be cooled, the technique is passive, economical, and does not cause any undue vibrations or noise in the system. However, the beneficial effect of an eddy promoter is maximized only if it is optimally located with respect to the object to be cooled. This sensitivity of thermal performance to geometrical arrangement has spurred considerable interest in identifying optimal component locations in ventilated enclosures.

† To whom correspondence should be addressed.

In this work, the flow and convective heat transfer characteristics of two relatively simple combinations of elements have been examined. Attention has been restricted to the two-dimensional, unsteady flows past pairs of cylinders of square cross-section aligned in tandem normal to the mean streamwise component of motion in a channel. While geometrically simple, as will be shown, the configurations investigated give rise to highly complex flows.

As a necessary background for understanding this class of bluff body flows, the first part of this investigation considers the fundamental case of two identical cylinders, with variable inter-cylinder spacing. Henceforth, this is referred to as problem A-A. The second part of the investigation addresses a more practical case, referred to as problem B-A, wherein the cross-sectional areas of the cylinders differ. In this case, the larger cylinder is heated and placed downstream of a smaller adiabatic cylinder. Flow visualization was performed for both problems A-A and B-A to provide fundamental qualitative insight into the structure of these flows, as well as to obtain information about the transitions between different modes of motion as a function of the inter-cylinder spacing and the Reynolds number. Numerical calculations were then performed for both cases to obtain more complete quantitative pictures of the flow fields, as well as the thermal solution for the second problem.

NOMENCLATURE

A	area [m^2]
C_D	drag coefficient, $2F_D/\rho U^2 A$
d	upstream cylinder diameter [m]; ($d = D$ for problem A-A)
D	downstream cylinder diameter [m]
f	eddy shedding frequency [Hz]
F_D	drag force [N]
g	acceleration due to gravity [m s^{-2}]
Gr	Grashof number, $g\beta(T-T_{ref})D^3/\nu^2$
h	heat transfer coefficient [W m^{-2} K^{-1}]
H	channel height [m]
k	thermal conductivity [W m^{-1} K^{-1}]
L	cylinder separation distance [m]
Nu	Nusselt number, hD/k
p	pressure [N m^{-2}]
q''	heat flux [W m^{-2}]
Re	Reynolds number, UD/ν
St	Strouhal number, fD/U
t	time [s]
T	temperature [K]
u	streamwise velocity component [m s^{-1}]
U	bulk average velocity [m s^{-1}]
v	transverse velocity component [m s^{-1}]
x	streamwise coordinate direction [m]
y	transverse coordinate direction [m].

Greek symbols

β	volume expansion coefficient, $\beta = 1/T_{ref}$ [K^{-1}]
δ	channel wall boundary layer thickness [m]
λ	non-dimensional cylinder separation, $\lambda = L/D$
μ	fluid viscosity [kg m^{-1} s^{-1}]
ν	fluid kinematic viscosity [m^2 s^{-1}]
ρ	fluid density [kg m^{-3}]
ω	vorticity [s^{-1}].

Subscripts

c	critical value
ref	reference value.

Superscripts

—	time average.

Other symbols

$\langle\ \rangle$	single surface average
$\langle\langle\ \rangle\rangle$	total surface average.

2. LITERATURE REVIEW

The background for this work includes previous investigations of the flow past single cylinders of square and rectangular cross-section. Experimental results for the Strouhal numbers of square and rectangular cylinders were presented by Okajima [1] for a range of Reynolds numbers spanning 70–20 000. For the unconfined square cylinder, Okajima recorded a slight and continuous decrease in Strouhal number with increasing Reynolds number over the range $200 \leqslant Re \leqslant 1000$. Above $Re = 1000$, the Strouhal number assumed a nearly constant value of 0.13. Corresponding numerical work performed by Davis and Moore [2] demonstrated the same variation of Strouhal number with Reynolds number, yielding a constant value of 0.14 for flows with $Re > 1000$. Davis *et al.* [3] reported that for a square cylinder confined to a channel, the coefficient of drag and the Strouhal number increased with increasing channel blockage ratio. The results from the latter study suggest that the Strouhal number is sensitive to the channel inlet flow conditions. Igarashi [4–6] and Goldstein *et al.* [7] experimentally investigated the flow and heat transfer from individual rectangular cylinders. They reported Nusselt numbers larger by almost 40% than those calculated using Hilbert's correlation (see Incropera and De Witt [8]), pointing to the need to use this relation cautiously.

The flow past identical circular cylinders in tandem has received some attention because of its wide practical applicability and associated stability issues. A review article by Zdravkovich [9] summarizes previous work on the subject. The research surveyed reveals the existence of two distinct flow patterns above and below a critical cylinder separation of 3.5 diameters, from center to center, over a wide range of Reynolds numbers. At low separations a vortex street is observed only in the wake of the downstream cylinder and the flow in the gap between the cylinders is essentially stagnant. In this range the pressure at the rear of the upstream cylinder increases with increasing cylinder spacing, thus reducing the drag on the upstream cylinder. The gap side of the downstream cylinder has a very low negative pressure (called the gap pressure), corresponding to the value of the upstream cylinder's base pressure. This produces a negative drag or a thrust force on the downstream cylinder. As cylinder separation increases, gap pressure increases, and the thrust force on the downstream cylinder decreases. Beyond the 3.5 diameter separation, vortex shedding by the upstream cylinder is also observed. This causes the gap pressure to jump to a significantly higher value, exceeding for the first time the value of the base pressure. Thus, a discontinuous increase in the drag coefficient of the downstream cylinder is registered. At this separation there is also a sudden drop in the base pressure which produces a positive jump in the drag on the upstream cylinder. The authors in Zdravkovich [9] comment on the bistable nature of the phenomenon, noting the intermittent display of both characteristic behaviors for a range of spacings centered around the critical spacing. They also observed that eddy shedding from the upstream cylinder strongly affects and synchronizes eddy shedding from the downstream cylinder.

A study of the aerodynamic instabilities of solid structures in tandem was performed by Shiraishi *et al.* [10]. For the case of two rectangular cylinders in tandem with a height to width ratio of 2, they found that the Strouhal number of the downstream cylinder decreased with increasing separation distances (measured from the upstream face of the upstream cylinder to the downstream face of the downstream cylinder) up to a critical separation of 4 cylinder heights. Above this separation the Strouhal number increased with the spacing ratio until it reached the value for the wake of a single cylinder corresponding to $St = 0.13$.

In experimental studies, Hiwada *et al.* [11] investigated the effects of placing two circular cylinders in tandem on the heat transfer from the downstream cylinder for different diameter ratios and inter-cylinder separations. They show that there is an optimal location for the upstream cylinder such that the Nusselt number for the downstream cylinder is maximized. They provide empirical correlations for the critical separation at which the upstream cylinder begins to shed eddies and for the location at which there is maximum heat transfer from the downstream cylinder. For $Re = 5\times10^4$, the critical clearance was found to be given by the correlation $1.5d+1.005D$ for $0.13 \leqslant d/D \leqslant 0.52$ and the clearance for which heat transfer was maximized was found to be $1.005D-1.5d$ for the same range of diameter ratios. Ota *et al.* [12] show similar results for elliptical cylinders.

Previous studies of bluff body flows have not yet provided a detailed description of the flow past a pair of cylinders of square cross-section in tandem, particularly for the flow in the inter-cylinder gap. Also lacking is a numerical investigation of this configuration. While heat transfer studies have produced information for circular cylinders in tandem, to our knowledge the case of square cylinders has not yet been adequately considered. Since arrangements of square cylinders correspond to geometries of considerable fundamental interest and practical utility, this study has focused on their experimental and numerical investigation over a Reynolds number range for which, as in Davis *et al.* [2, 3], direct numerical simulations are possible.

3. EXPERIMENTAL APPARATUS, PROCEDURE AND UNCERTAINTIES

Flow visualization was performed using a dye injection technique in a water channel. A closed loop system provided a constant head flow into a Plexiglas test section, 81 cm long, 6.6 cm high, and 30.5 cm wide. A flow conditioning section preceding the inlet to the test section ensured a homogeneous uniform steady flow. The channel test section and associated flow system are described in full detail by Treidler [13].

Two cylinders, each of square cross-section, were positioned in tandem perpendicular to the flow, as shown in Fig. 1(a). For problem A-A, the two cylinders were identical in size, with square cross sections of 12.7×12.7 mm^2. For problem B-A, the downstream cylinder was 12.7×12.7 mm^2 in cross-section, while the upstream cylinder was 6.35×6.35 mm^2 in cross-section. For both problems the cylinders were centered on the channel mid-plane, and spanned the width of the channel. Brackets were used to support the cylinders at their ends while allowing a continuous adjustment of the horizontal distance between them. Each cylinder was constructed of clear acrylic, with a duct machined along its length to contain dye. The dye was gravity fed into a cylinder via a port at one end of its duct. For each cylinder, a slit in its upstream face allowed the injection of dye into the channel flow at the forward stagnation point of the cylinder. This slit was 2.5 cm long and 1 mm wide, and was centered lengthwise and heightwise on the cylinder wall. The upstream cylinder was supplied with a dilute solution of methylene blue in water, and the downstream cylinder was supplied with a dilute solution of red food coloring in water.

For the A-A experiments, flow visualization was performed for cylinder separations of 0.25–4.0D over a range of Reynolds numbers spanning 200–1600. In the B-A experiments, inter-cylinder spacings of $2D$ and $3D$ were considered for Reynolds numbers spanning 185–464. Separation distances were set using a micrometer, and extreme care was taken to align the cylinders symmetrically with respect to the channel mid-plane and perpendicular to the bulk flow. The experimental apparatus was allowed to stand for a minimum of 48 h prior to experimentation, to allow the water and dye solution temperatures to equilibrate with the ambient. For each cylinder separation, the flow rate was varied from low to high Reynolds numbers through the entire range. Still photography and video recordings were performed for problem A-A with the cameras facing the side wall of the test section, in line with the cylinders, to record the flow between and around the cylinders. Video recordings only were performed for problem B-A and, as a consequence, these results are not presented here but are used to interpret the numerical calculations performed for problem B-A. In both cases, special care was taken to control the rate of dye injection so as to minimize any adverse effects on the motion of fluid between and past the cylinders.

To check whether the injection of dye affected the flow, the behavior with a low rate of injection of dye into the system was compared to the behavior observed when a small amount of dye remained in the recirculation areas to mark the flow but no new dye

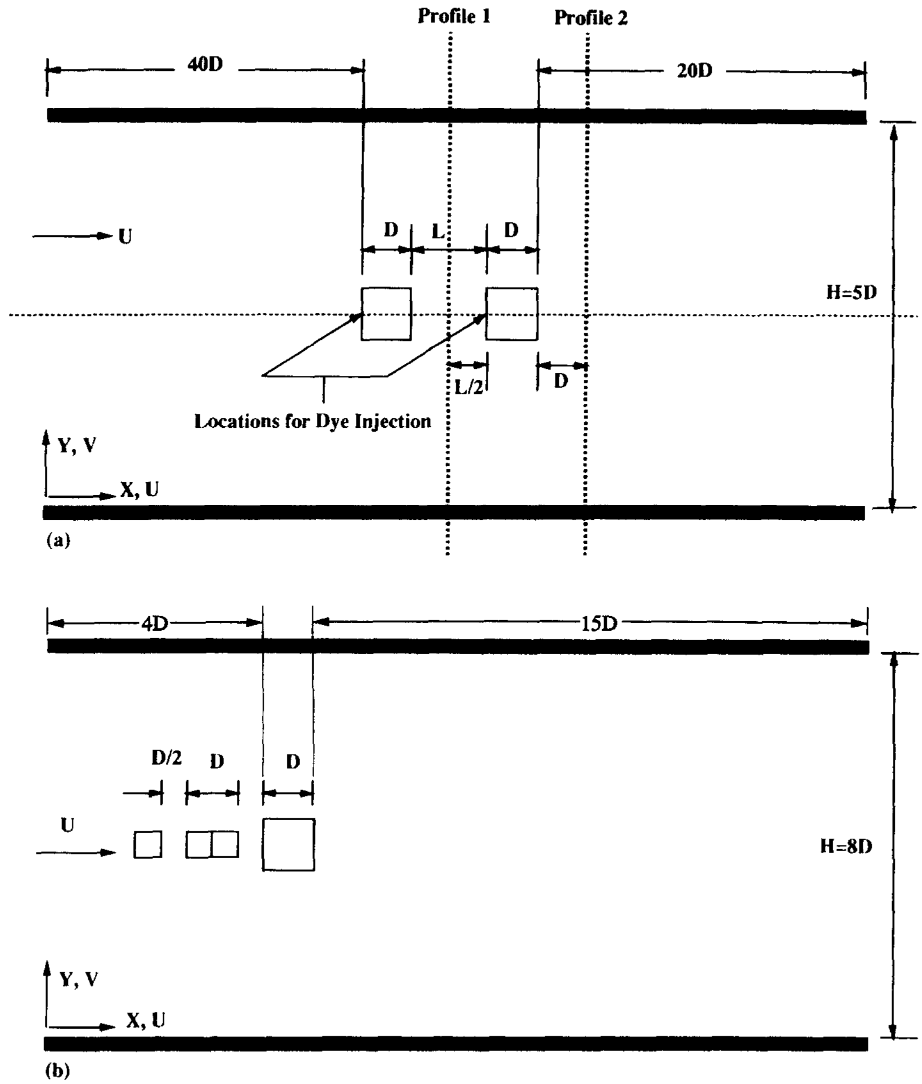

FIG. 1. Flow configuration for experimental visualization of problem A-A (a) and numerical calculation of problem B-A (b). Schematic defining coordinate system and relevant dimensions. In (a) vertical planes indicate positions for which calculated velocity profiles are shown in Fig. 9. In (b) three positions for the upstream eddy promoter are shown.

was being injected. This comparison revealed that for a small steady flow of dye into the channel, no interference with the flow pattern resulted. A visual check for the buoyancy of the dye solutions was performed in still water. The blue dye was found to be neutrally buoyant but the red dye was found to be slightly heavier than the channel water. However, only for the lowest Reynolds numbers investigated did the tendency of the red dye to sink cause a minor asymmetry from top to bottom in the structures observed in the inter-cylinder recirculation region. For $Re > 400$ the buoyancy-induced asymmetry was not detectable.

From views of the flow through the top of the test section during a run, it was ascertained that no significant spanwise motion existed in the wake downstream of the second cylinder. Three-dimensionality was observed in the inter-cylinder recirculation region but even in this region no systematic spanwise structures were noted. Thus, the flow was considered to be two-dimensional on average for the purposes of this study, and this is the way we have interpreted the side (spanwise integrated) views recorded photographically.

The Reynolds number of the flow was known to within 4% r.m.s. with the main source of uncertainty due to the measurement of the bulk velocity. The non-dimensional gap width was known to better than 2% r.m.s. The visual measurement of wake periodicity yielded a Strouhal number with a total uncertainty of 5.8% r.m.s.

4. NUMERICAL PROCEDURE

Direct numerical simulations of the flow were performed using the CUTEFLOWS numerical calculation algorithm. The code is based on the successive dissertations of Schuler [14] and Treidler [13]. It is documented in detail in these references and in Schuler *et al.* [15] and Humphrey *et al.* [16]. The numerical algorithm features a modular format that allows conditional compilation for problem definition and modification, and is implemented with the Unix operating system utilities and the NCSA HDF graphics facilities in mind.

CUTEFLOWS (Computing Unsteady Three-dimensional Elliptic Flows) is a finite-difference type algorithm that explicitly computes the time evolution of the primitive variables (u, v, w, p, and T) of fully 3-D (and, in the present case, 2-D) incompressible unsteady flows. The spatial discretization of the Navier–Stokes and continuity equations is based on a staggered grid control volume formulation. It employs a second order accurate (QUICK) scheme for the convection terms and central differencing for diffusion terms. A second order accurate Runge–Kutta predictor–corrector scheme (RK2) is used to solve the resulting set of time-dependent ordinary differential equations for the velocity components at their respective grid locations. To accomplish this, the divergence-free velocity field at each new time step is decomposed, as explained by Chorin and Marsden [17], into a pseudo-velocity field independent of pressure and a separate pressure contribution. Using the RK2 algorithm, the pressure-less pseudo-velocity is computed directly. The pressure contribution is defined by the discrete Poisson equation that results from the imposition of the divergence-free condition on the velocity field. This contribution is calculated at the end of each half-time step using the conjugate gradient method. A much more detailed account of the numerical algorithm and of the rigorous testing it has undergone is given in the above-mentioned references.

4.1. *Calculation boundary conditions*

Problem A-A. For this problem, except for the inlet and outlet plane locations discussed below, the geometrical configuration calculated corresponds to that shown in Fig. 1(a), and essentially matches the flow visualization experiment. For the calculations, the physical properties of water at 300 K were used. The two-dimensional calculation domain is bounded at the top and bottom by the fixed channel walls. Estimates of the channel wall boundary layer thickness, δ, at the x-location corresponding to the upstream cylinder yielded $\delta = 0.9D$ for $Re = 800$ and $\delta = 1.3D$ for $Re = 400$. However, in order to simplify the calculations, and to test the dependence of the flow on interactions with the channel walls, the u velocity component along these walls was set to $u = U$, the value of the inlet velocity, and $v = 0$ was imposed. Physically, this translates into sliding wall boundary conditions. At the channel inlet $u = U$ and $v = 0$ were uniformly prescribed, corresponding to a plug flow velocity profile. At the outlet, the wave equation condition discussed and used by Arnal *et al.* [18] was employed. This condition, also known as the Sommerfeld radiation condition, states that

$$\frac{\partial \phi}{\partial t} + \frac{\partial (u\phi)}{\partial x} = 0 \qquad (1)$$

where ϕ represents the quantity conserved, in this case u. The use of equation (1) allows the vortices shed by the cylinders to emerge from the computational domain with a minimal distortion to the flow field, and without generating perturbations that reflect backwards into the upstream flow. No slip, impermeable wall boundary conditions for velocity were imposed along all cylinder surfaces.

The use of sliding wall boundary conditions at the top and bottom channel walls is highly desirable because it reduces the grid refinement necessary to resolve the thicker boundary layers that would arise for fixed channel walls. This way it is possible to concentrate the calculation mesh around the cylinders where the unsteady flow is of much more interest. To test the effect of the artificial sliding walls condition, a case was computed using the fixed wall boundary conditions, all other parameters being the same. This computation, performed on an identical grid with ($x = 124$, $y = 72$) nodes, yielded results for the flow about the cylinders essentially identical to those calculated for the corresponding sliding walls case. The implication of this comparison is that, for the conditions investigated, the experimental flow is predominantly a function of the cylinder–cylinder interactions, and it is concluded that the inter-cylinder flow is not significantly affected by the boundary layers developing along the fixed channel walls. Thus, while in the experiment the distance between the inlet plane and the upstream cylinder was $40D$, through trial and error we found that fixing a value of $4D$ with the sliding walls condition was sufficient for all the Re calculated to accurately simulate the plug flow velocity condition approaching the cylinders. Similarly, the use of equation (1) at the exit plane allowed us to place this plane at a distance 7–$21D$ from the downstream cylinder, depending on the Reynolds number, without significantly affecting the inter-cylinder flow.

Problem B-A. For this case, the calculated geometry is shown in Fig. 1(b), and the physical properties of air at 300 K were used. Both the geometry and fluid used for the calculation differ from the corresponding experiment for which water was used. Notwithstanding, the flow visualization results have helped to interpret the present numerical findings.

For this problem, a plug flow velocity profile ($u = U$) was specified at the inlet plane, $4D$ ahead of the downstream cylinder, and equation (1) was used at the outlet, $15D$ behind the downstream cylinder. The value of $v = 0$ was also specified at these planes. No slip, impermeable wall boundary conditions for velocity were imposed at the top and bottom channel walls and along all cylinder surfaces. For temperature, a uniform value of $T = 300$ K was fixed at the inlet plane and equation (1) with $\phi = T$ was specified at the outlet. The top and bottom walls of the channel were prescribed as adiabatic, as was the upstream small cylinder. The larger downstream cylinder was fixed to dissipate heat from each of its four surfaces at the fixed rate of $q'' = 5\ \mathrm{W\ m^{-2}}$.

For both problems A-A and B-A initial flow fields (and for problem B-A, temperature fields also) were prescribed at $t = 0$ to accelerate the establishment of steady, periodic solutions.

4.2. *Grid refinement, time step considerations and testing*

Previous work reported by Treidler [13] for the flow past arrays of square cylinders for the same range of Reynolds numbers considered here permits an a priori estimation of the number and distribution of grid nodes required to resolve the present flows. The computational domain in problem A-A was $5D$ high in the y-direction, and varied in the x-direction, from $14D$ to $28D$, depending on the length necessary to avoid negative u velocities at the outlet plane. Corresponding to the necessary length, the total number of nodes varied from ($x = 124$, $y = 72$) to ($x = 208$, $y = 72$). The calculation for this problem case used a non-uniform grid in the x-direction and a uniform grid in the y-direction, with a greater concentration of nodes around the cylinders and gap region than in the upstream or downstream regions. For a section of the calculational domain beginning one diameter upstream of the first cylinder and ending two diameters downstream of the second cylinder, the grid was twice as refined in the x-direction than it was for the rest of the domain. This arrangement guaranteed a grid density of 12 nodes per cylinder diameter in both the x- and y-directions in the inter-cylinder region. For problem B-A, the domain was typically $20D$ long in the x-coordinate direction with 92 grid nodes and $8D$ high in the y-coordinate direction with 48 grid nodes. The grids were refined near to the cylinder surfaces and near the channel walls, to give a grid density of 8 nodes per cylinder diameter (D).

To check grid independence, numerical simulations of problem A-A were performed on grids that were 50% more refined and 50% less refined, respectively, than the final grid used. The tests were conducted for a cylinder separation of 1.5 diameters at a Reynolds number of 800. The most refined grid (18 nodes per cylinder diameter) yielded a Strouhal number, an average drag coefficient for the upstream cylinder, and an average drag coefficient for the downstream cylinder that differed by 0, 4, and 2%, respectively, from the values computed on the intermediate grid used in the investigation. The time records of the lift coefficients computed on the refined and intermediate grids were also in good qualitative agreement. The coarser grid calculation yielded iso-vorticity and streamline contour plots in qualitative agreement with the results of the intermediate grid, but produced a 16.6% error in the Strouhal number. From these and related observations for the velocity components it was concluded that the grids finally chosen for computation of the two problem cases yielded results numerically accurate to better than 5% in the field variables.

The time step for the calculations was chosen as 0.001 s. Computations carried out with a time interval twice this size yielded identical results, thus demonstrating the independence of the results on the time step parameter. At much larger time steps (0.01), the calculations were found to be unstable due to the explicit nature of the algorithm.

CUTEFLOWS has been used successfully to accurately compute a variety of flow configurations; most notably the unsteady flow between co-rotating disks in enclosures (Schuler [14]), and unsteady flows past bluff bodies in channels (Treidler [13]) including, as a limiting case, the configuration investigated by Davis and Moore [2].

Further testing has been performed more recently by Tatsutani *et al.* [19]. This consisted in implementing CUTEFLOWS for the case of two-dimensional flow through a channel with a backward facing step. A parabolic velocity profile was specified at the inlet and the wave boundary condition was specified at the outlet while $u = v = 0$ were fixed along the channel walls. The results of that work are in excellent agreement with the results established by Gartling [20].

5. RESULTS AND DISCUSSION

Problem A-A: flow visualization

A representative sample of the flow visualization still photographs available in Tatsutani and Humphrey [21] is presented here. At the lowest visualized flow rate ($Re = 200$) the flow is dynamically similar over the entire range of cylinder separations. Activity in the inter-cylinder region is limited to a pair of opposite signed vortices or eddies with rotational directions fixed by the flow in the free stream at the top and bottom of the inter-cylinder recirculation region. Virtually no exchange of fluid occurs between the water in the inter-cylinder gap and the free stream. In this sense, the fluid in the gap can be considered to be recirculating but stagnant.

A second flow pattern characterizes the range of cylinder spacings going from 0.25 to 1.5 diameters, over the range of Reynolds numbers spanning 400–1600. In the visualization of a flow at $Re = 400$, there are visible striations in the dye marking the counter-rotating vortices in the gap. This is indicative of the periodic intake of a minor amount of fluid from the wake of the upstream cylinder (marked by blue dye). With an increasing Reynolds number at these separation distances, it is observed that the fluid in the gap becomes substantially more unsteady and mixed. Typical flow visualization results are shown in Figs. 2(a) and (b). For these conditions, an oscillating vertical bulk displacement of the fluid in the inter-cylinder gap, and a significant distortion of the two vortex structures, are observed in both the flow visualization and the numerical simulations. Small but

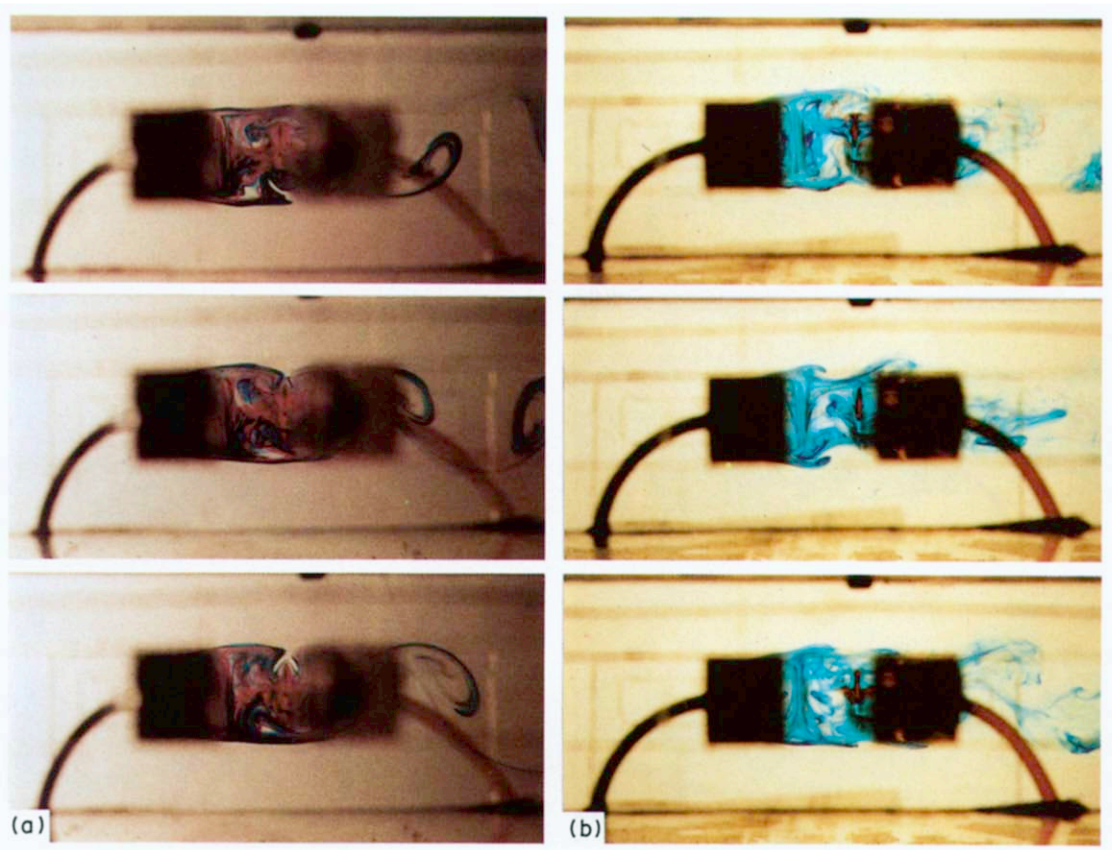

FIG. 2. Visualization of the flow of water past a pair of square cylinders in a channel: $\lambda = 1$; (a) $Re = 800$; (b) $Re = 1200$.

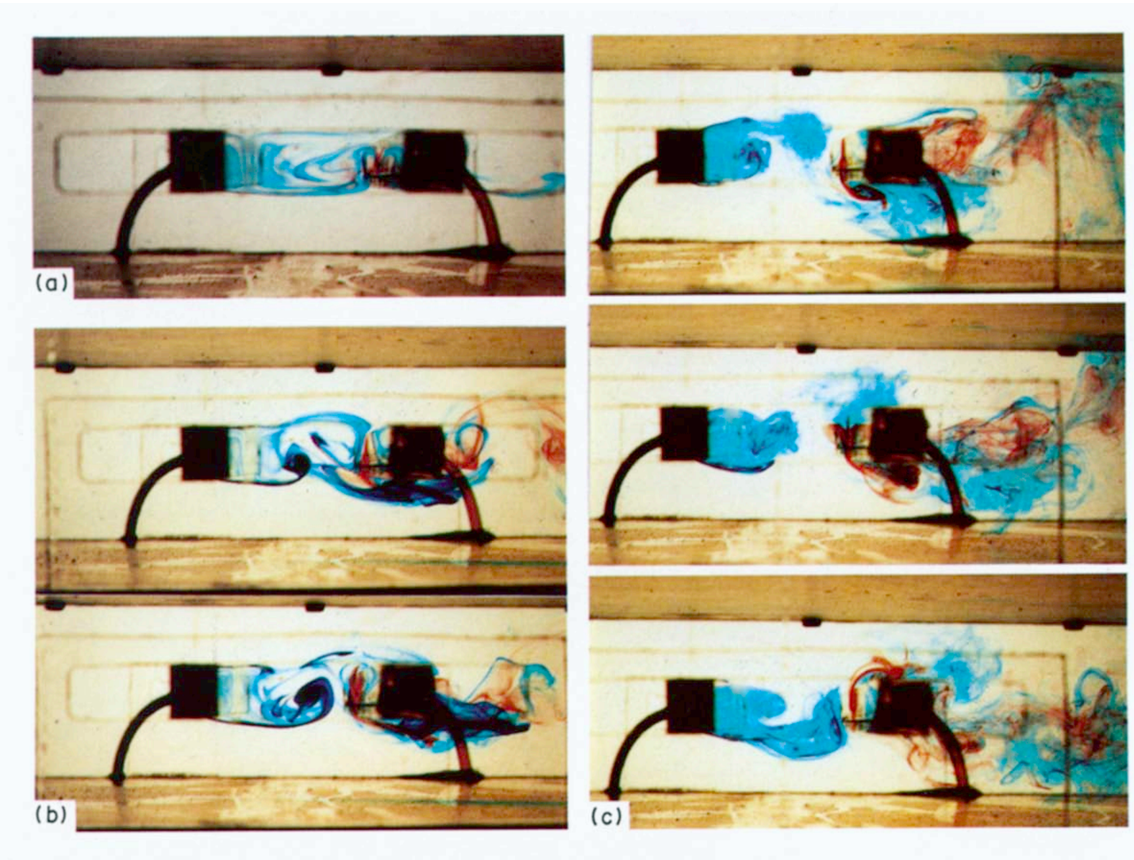

FIG. 3. Visualization of the flow of water past a pair of square cylinders in a channel: $\lambda = 3$; (a) $Re = 320$; (b) $Re = 400$; (c) $Re = 800$.

intense jets of water alternately penetrate into the gap recirculation region from the top and bottom horizontal surfaces of the downstream cylinder. These periodic back-flowing wall jets significantly disrupt the two vortex structure in the gap, and in some cases are seen to establish a second set of vortices with opposite rotation to the original set. The periodicity of the bulk vertical motion and of the alternating back-flowing jets agrees with the frequency of eddy shedding from the downstream cylinder. This suggests that the driving mechanism for these two phenomena is the periodic variation in the vertical pressure gradient created, primarily, by the oscillating wake of the downstream cylinder. As the cylinder spacing increases within this range, the periodic displacement of fluid in the gap and the appearance of the alternating jets is observed at consecutively lower Reynolds numbers.

A third flow pattern is observed experimentally and numerically at even larger cylinder separation distances. Considering $\lambda = 3.0$ as a representative case, visualization of a low Reynolds number flow ($Re = 300$) reveals the previously described steady two-vortex recirculation structure in the inter-cylinder gap. At a higher Reynolds number ($Re = 320$) a condition is observed wherein the recirculation region remains essentially intact but for which periodic intakes of free stream fluid, in the form of the back-flowing jets, occur. However, this condition appears only over a narrow range of Reynolds numbers and appears to be unstable. With a small further increase in Reynolds number, a transition to an entirely new behavior is observed. This is shown in Figs. 3(a), (b), and (c) for $Re = 320$, 400, and 800, respectively. Now the recirculation region no longer exists between the two cylinders. Instead, vortex sheets are alternately shed by the upstream cylinder and these travel diagonally through the gap, washing across the upstream face of the downstream cylinder. Thus, the upstream surface of the downstream cylinder is exposed to a periodic flushing condition induced by the upstream cylinder.

During the visualization, the point of transition for the behavior described in the preceding paragraph varied from run to run over a considerable range of Reynolds numbers and appeared to be sensitive to any unsteadiness in the flow. For values larger than the critical spacing, the eddy shedding from the upstream cylinder was stabilized.

Problem A-A: numerical results

Extensive numerical calculations for problem A-A are given in Tatsutani and Humphrey [21]. Three numerical pictures of the flow are presented here as iso-vorticity contour plots. Figure 4 shows that for $\lambda = 1.5$ with $Re = 800$, both the periodic ingestion of backward-jetting fluid from the downstream cylinder top and bottom walls, and the periodic formation of additional vortices at the leading edges of this cylinder, are predicted by the numerical simulation. Figures 5 and 6 present numerical predictions of the formation of the vortex street in the wake of the upstream cylinder for $\lambda = 3.0$ with $Re = 400$ and $Re = 800$, respectively. The numerical simulation of the first case verifies that close to the transition point the flow is bistable, in the sense that it alternates between the two patterns observed experimentally; one with a closed gap recirculation region, the other with an oscillating wake forming behind the upstream cylinder. The numerical simulation captures both of the flow patterns observed in the visualization, and predicts approximately equivalent transition points. The critical spacing, λ_c, for this transition is identified numerically as $\lambda_c = 3$ for $Re = 400$, $\lambda_c = 2$ for $Re = 800$, and close to $\lambda_c = 1.5$ for $Re = 1200$. Assuming $\lambda_c = a\,Re^b$, a fit to this data yields the relation $\lambda_c = 168\ Re^{-2/3}$ which predicts λ_c as a function of Re to better than 4%.

The numerically determined Strouhal numbers presented in Fig. 7(b) are in reasonable agreement with the experimental results presented in Fig. 7(a). A decrease in Strouhal number with increasing Reynolds number is evident for all separation distances except $\lambda = 2.5$. Over this range of Reynolds numbers the Strouhal number is inversely related to the cylinder separation. The results for lower separations ($\lambda = 0.5$–2.0) correspond well with the eddy shedding frequencies reported by Okajima [1] and Davis and Moore [2] for a single square cylinder.

The numerical simulation allows the calculation of time records of the lift and drag forces acting on the cylinders which are difficult to obtain experimentally. Time records of the lift coefficients, available in Tatsutani and Humphrey [21], show that the fluctuation amplitudes of the lift force experienced by the upstream cylinder are about 4 times larger in the range of separations $2 < \lambda < 3$ than in the range $0.5 < \lambda < 1.5$. For the downstream cylinder, the amplitudes are increased by a factor of approximately 5/2. This is explained in terms of the flow transition occurring at the $\lambda = 2$ cylinder separation. The onset of vortex shedding by the upstream cylinder induces large destabilizing forces on both cylinders. This is reflected in the increased instantaneous lift coefficients of the cylinders. For $Re \geqslant 800$, the lift and drag coefficient time records are chaotic for all cases because of the unsteady and non-linear nature of the cylinder interactions.

The results for computed drag coefficients are presented in Fig. 8(a). The data points represent time-averages over a minimum of ten periods for any case shown. These results are analogous to those reported for circular cylinders in tandem and suggest similar flow patterns. For Reynolds numbers of 800 and 1200, the upstream cylinder experiences a positive drag force that decreases slightly with increasing separation distance, up to the critical separation. This is attributed to the form of the variation of the gap pressure with cylinder separation. At low separations the low gap pressure enhances the drag force acting on the

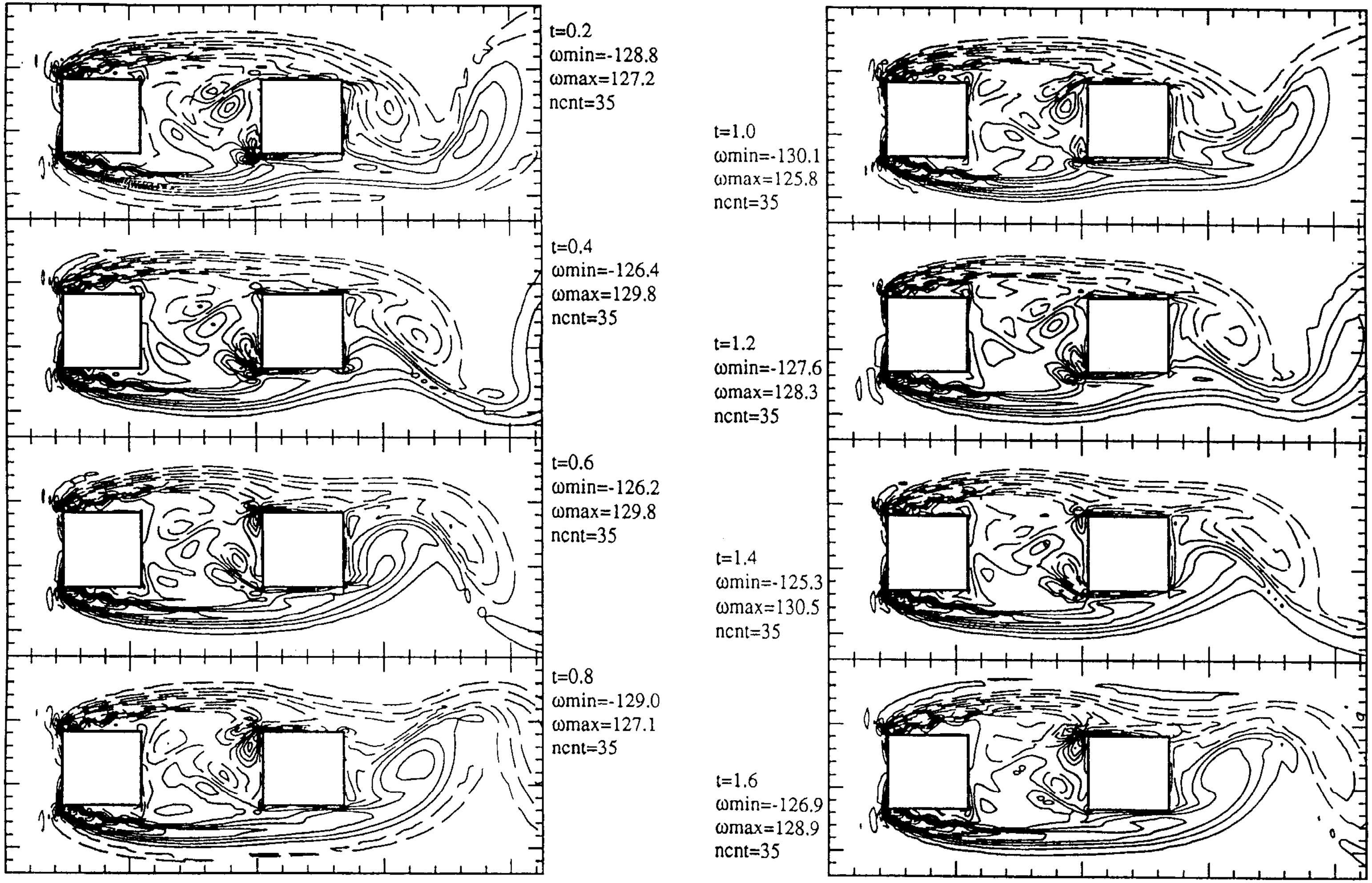

FIG. 4. Calculated isovorticity contours at 0.2 s intervals for $D/d = 1$ and $\lambda = 1.5$ with $Re = 800$. View shown is restricted to region immediately around the cylinders.

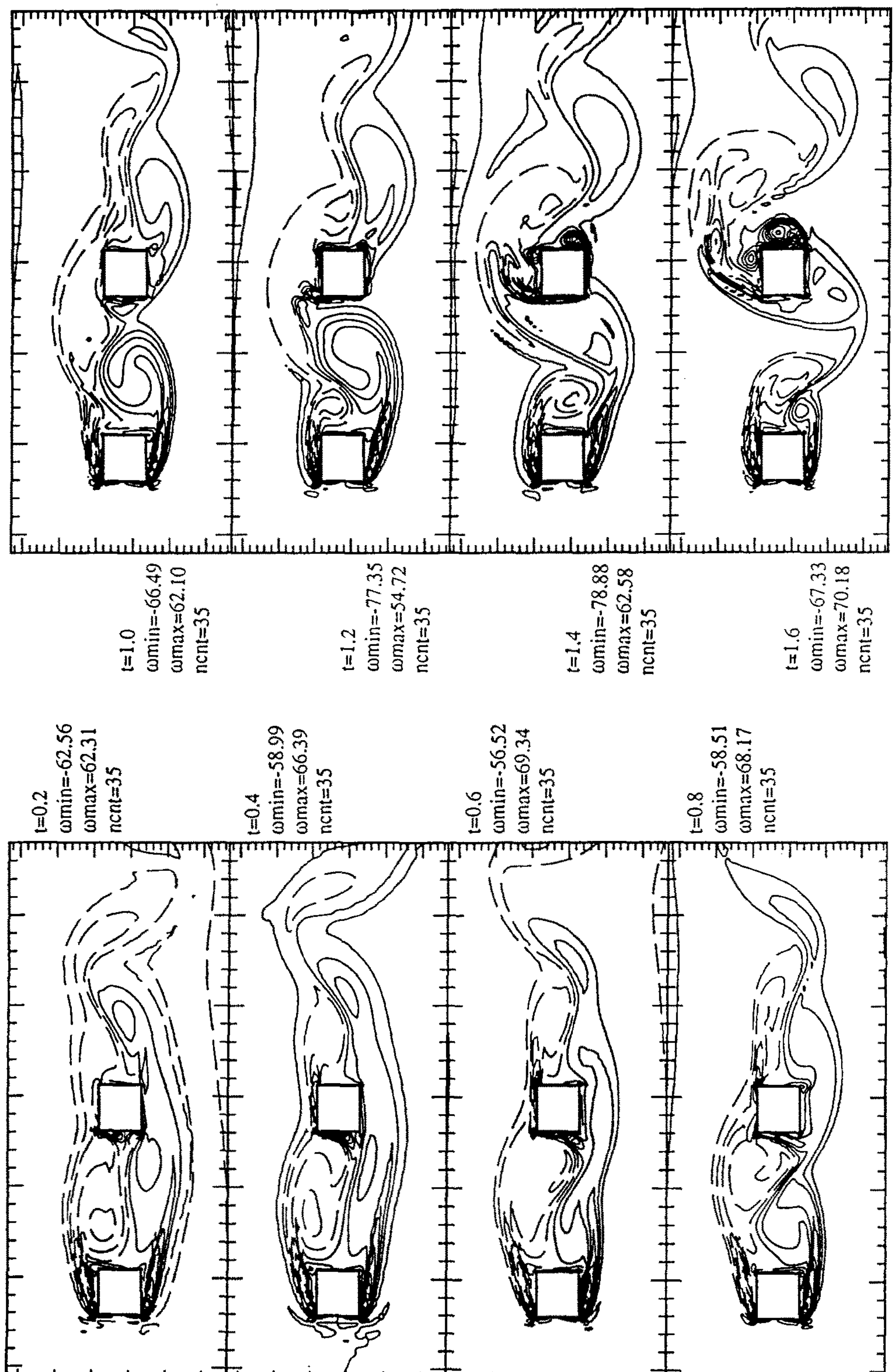

FIG. 5. Calculated isovorticity contours at 0.2 s intervals for $D/d = 1$ and $\lambda = 3$ with $Re = 400$. View shown is restricted to region immediately around the cylinders.

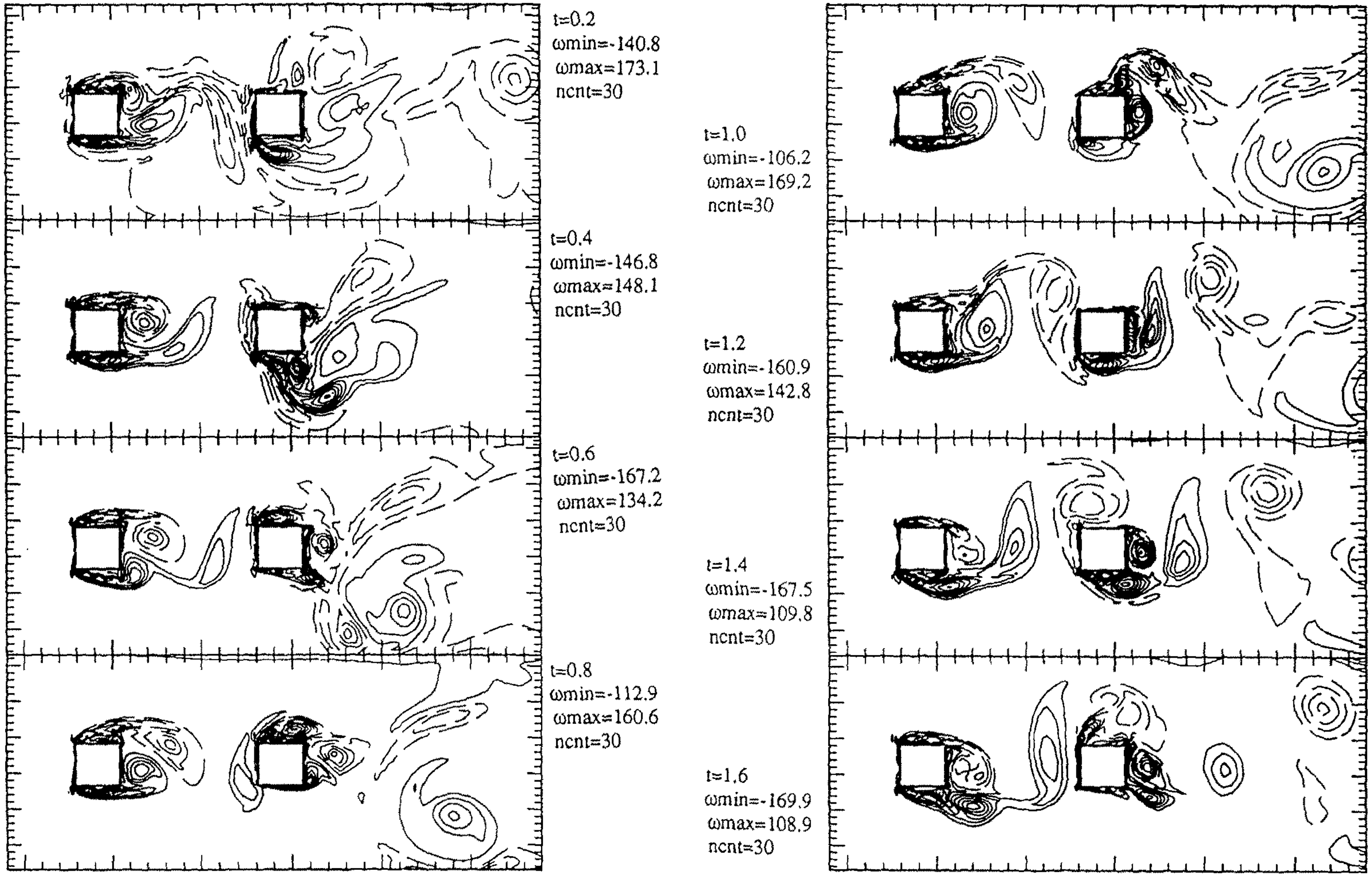

FIG. 6. Calculated isovorticity contours at 0.2 s intervals for $D/d = 1$ and $\lambda = 3$ with $Re = 800$. View shown is restricted to region immediately around the cylinders.

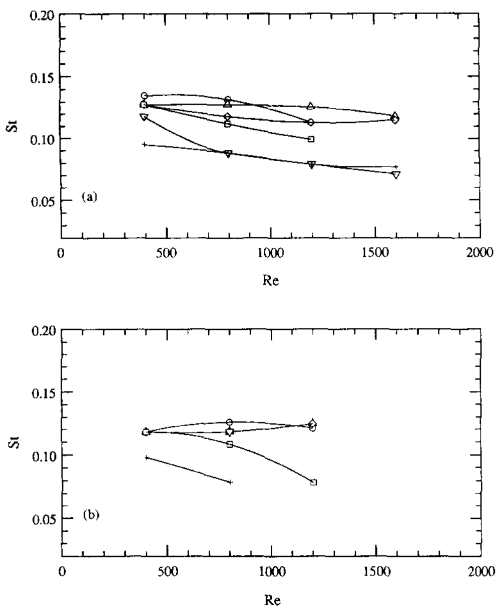

FIG. 7. Measured (a) and calculated (b) Strouhal number vs Reynolds number: $\lambda = 0.5$ (○), $\lambda = 1.0$ (△), $\lambda = 1.5$ (◇), $\lambda = 2.0$ (□), $\lambda = 2.5$ (▽), $\lambda = 3.0$ (+).

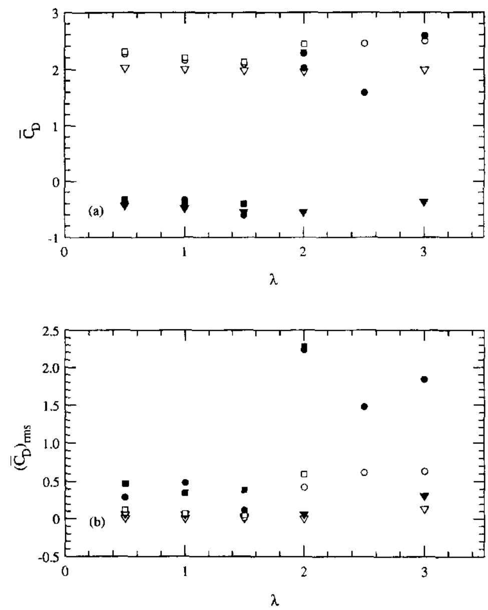

FIG. 8. Calculated time averaged drag coefficients (a) and their r.m.s. (b) vs cylinder separation distance. Blank symbols represent data for upstream cylinder, filled symbols represent data for downstream cylinder. Case 1: $Re = 400$ (▼), case 2: $Re = 800$ (●), case 3: $Re = 1200$ (■).

upstream cylinder. As the gap pressure increases with separation, the total drag on the upstream cylinder decreases. At the critical separation, which marks the commencement of vortex shedding by the upstream cylinder, an inflection in the curve is observed and the drag coefficient subsequently increases with separation. At these Reynolds numbers a large discontinuity is observed in the drag on the downstream cylinder. Below the critical separation the low gap pressure causes a negative drag or thrust force on the cylinder. At the critical separation a discontinuous positive jump in the average drag coefficient of the downstream cylinder occurs. Beyond this point the drag increases to a value equivalent to the drag on the upstream cylinder. Thus the formation of a wake behind the upstream cylinder causes a dramatic increase in the normal and shear forces experienced by the downstream cylinder.

For lower Reynolds number flow ($Re = 400$ with $\lambda < 3$), eddy shedding from the upstream cylinder is not observed in the calculations. The recirculation region remains closed, producing a continuous decrease in the drag force on the upstream cylinder with increasing separation distance, as explained above. Also, due to the low gap pressure associated with the existence of the recirculation region, the downstream cylinder experiences a relatively constant thrust force over the entire range of separations.

The r.m.s. of the average drag coefficients is plotted against separation distance in Fig. 8(b). This figure reveals that the average fluctuation of drag about the mean is uniformly greater for the downstream cylinder than for the upstream cylinder. Another trend demonstrated by this plot is that the r.m.s. varies directly with Reynolds number. The discontinuity noted in Fig. 8(a) is also evident in Fig. 8(b), with a sudden increase in the r.m.s. of the drag coefficient of the downstream cylinder, and a positive inflection in the r.m.s. curve for the upstream cylinder. Thus, the commencement of eddy shedding by the upstream cylinder induces increased fluctuations in the drag coefficients of both cylinders.

Figure 9 presents detailed u-velocity profiles calculated for separations of 1, 2, and 3 diameters at $Re = 800$. The profiles correspond to the two streamwise locations indicated in Fig. 1(a) and, in each plot, represent the flow at four distinct instants in time, separated by 0.4 s intervals. These results quantitatively demonstrate the unsteadiness of the flow between the cylinders and in the wake of the downstream cylinder. For $\lambda = 1$, the velocity profile between the cylinders experiences relatively limited variations with time, while the wake velocity profile fluctuates significantly with time. At higher separations, especially for $\lambda = 3$, the velocity profile between the cylinders also fluctuates significantly with time, and the time variation of the profile in the wake is enhanced. These results provide a final measure of the increasing unsteadiness of the flow with increasing cylinder separation, particularly in the inter-cylinder gap.

Problem B-A: experimental and numerical results

Numerical results were also calculated for the flow and heat transfer involving a single square heated cylinder, and for the same cylinder with a smaller

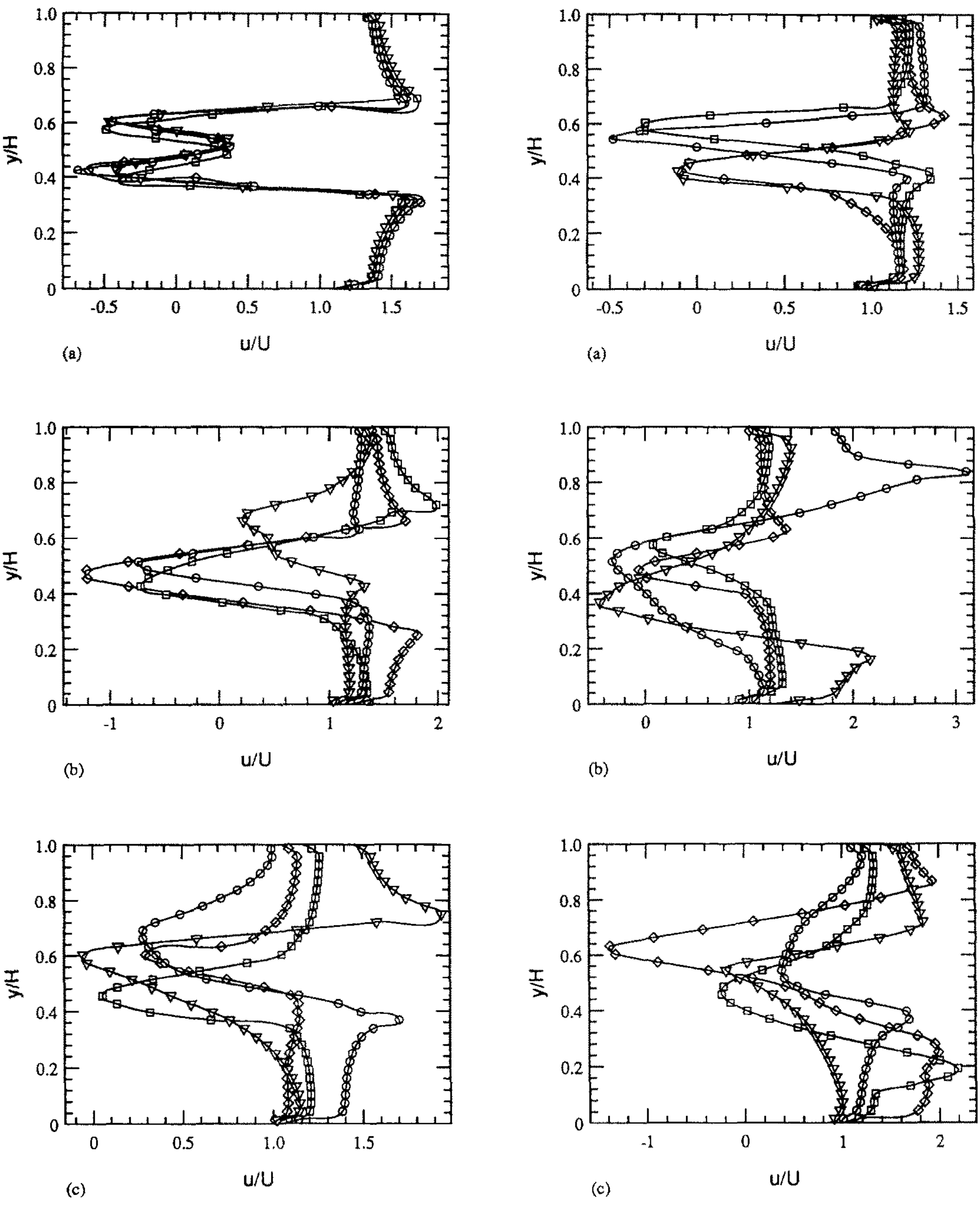

FIG. 9. Horizontal velocity component profiles at two streamwise locations for $\lambda = 1.0$ (a), $\lambda = 2.0$ (b), and $\lambda = 3.0$ (c) at $Re = 800$. Plots on the right show velocity profiles midway between the cylinders; plots on the left show velocity profiles one cylinder diameter behind the downstream cylinder, as indicated in Fig. 1(a). Profiles shown for four instants in time, at intervals of 0.4 s: $t = 0.4$ (◇), $t = 0.8$ (□), $t = 1.2$ (▽), and $t = 1.6$ (○).

adiabatic square cylinder or 'eddy promoter' placed in front of it. The calculated configurations of interest are shown in Fig. 1(b) and the values of the relevant parameters are: $D = 2$ cm, $d = D/2$, $H = 8D$ and $U = 0.5$ m s^{-1} yielding a value of $Re = 592$. The inlet flow was at 300 K and the highest calculated cylinder surface temperature was 412 K. Using a corresponding film temperature, the value of Gr/Re^2 was found to be 0.25. Thus the predominant mode of heat transfer was taken to be forced convection and buoyancy effects were neglected. (We remind the reader that in these calculations the channel walls are fixed.)

Single heated cylinder

For the case of a single heated cylinder of square cross-section, the Strouhal number was found to be 0.15. This value, as well as the calculations of the lift and drag coefficients, are in very good agreement with the results obtained by Davis *et al.* [3] for a similar flow configuration. These detailed comparisons are given in Devarakonda and Humphrey [22].

Figure 10(a) shows the single surface-averaged Nusselt number for each of the four surfaces of a single heated cylinder as a function of time. Except for small time scale variations due to stagnation point fluctuations on the upstream surface, the figure shows that the numerical solution has essentially reached steady periodicity. The upstream cylinder surface shows the highest Nusselt number. This is followed by the top, bottom and downstream surfaces, respectively. The Nusselt number variations for the top and bottom surfaces are not in phase but are identical in their respective detailed features. A fast Fourier transform of these sequences indicates that the dominant frequency corresponds to a Strouhal number of 0.15, the eddy-shedding frequency of the cylinder. Figure 10(b) shows corresponding plots for the single surface-averaged temperatures as a function of time. The time and total surface-averaged Nusselt number, $\langle\langle \overline{Nu} \rangle\rangle$, was determined from the time records of the single surface-averages by averaging over the four surfaces. The result was calculated to be 4.57. This result is less than the value 6.74 obtained using Hilbert's correlation (see Incropera and De Witt [8]), $Nu = 0.102\ Re^{0.675}\ Pr^{1/3}$ for $5 \times 10^3 < Re < 10^5$. The comparison is limited to the order of magnitude, since Hilbert's correlation is not necessarily valid for $Re \ll 5 \times 10^3$.

Heated cylinder with eddy promoter

Three inter-cylinder spacings were investigated wherein the smaller adiabatic cylinder was placed $0.5D$, $1D$ and $2D$ upstream of the larger heated cylinder with both cylinders aligned on the center of the channel. All three cases yielded a dominant eddy-shedding frequency corresponding to a Strouhal number of 0.25. This was observed even when there was no eddy shedding from the upstream cylinder and is a value considerably larger than the $St = 0.15$ for the single cylinder case.

Figures 11(a) and (b) show plots of the single surface-averaged Nusselt number and temperature for each of the four surfaces corresponding to the case with an inter-cylinder spacing of $\lambda = 0.5$. In contrast to the single cylinder results (Figs. 10(a) and (b)), with the upstream cylinder present both the magnitudes and r.m.s. of the temperatures at the top and bottom walls and at the downstream wall of the heated cylinder are significantly reduced. Now the top and bottom wall Nusselt numbers are larger than the value for the upstream surface which itself has been reduced. Notwithstanding, from the values of $\langle \overline{Nu} \rangle$ shown it is clear that the total Nusselt number, $\langle\langle \overline{Nu} \rangle\rangle$, is larger by 52% with the upstream cylinder in place. Clearly, the presence of the small cylinder has a significant effect on the heat transfer from the larger.

Figure 12 provides plots of time- and total surface-averaged Nusselt numbers and temperatures as a

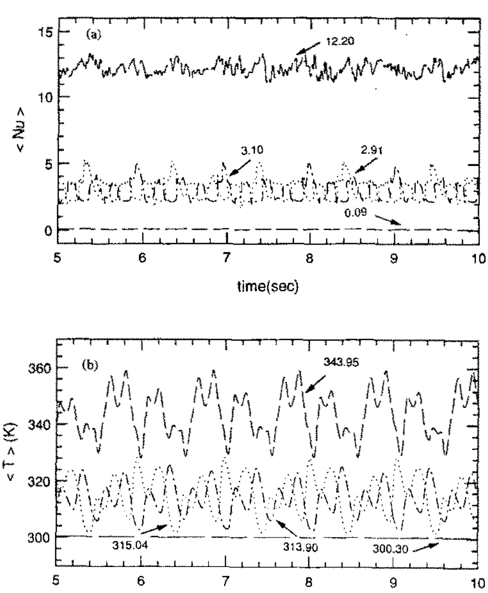

FIG. 10. Time records of single surface-averaged Nusselt number (a) and single surface-averaged temperature (b) for each of the four surfaces of a single heated square cylinder with $Re = 592$ in a channel flow. Inserts in (a) show time-averaged Nusselt number, $\langle \overline{Nu} \rangle$, and in (b) time-averaged temperature, $\langle \overline{T} \rangle$, for each surface: —— upstream face, ---- top face, — — downstream face, ······ bottom face.

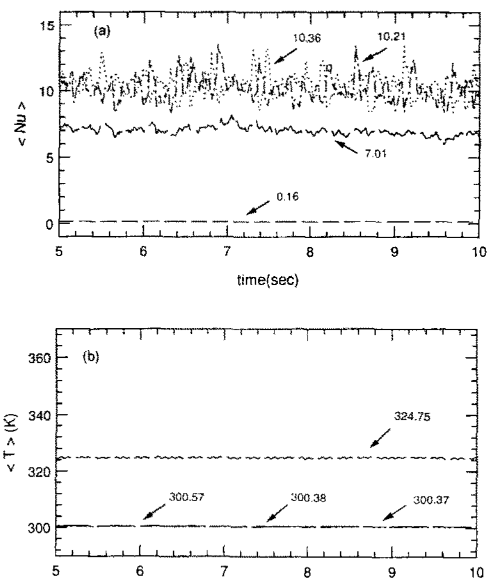

FIG. 11. Time records of single surface-averaged Nusselt number (a) and single surface-averaged temperature (b) for each of the four surfaces of a heated square cylinder with $Re = 592$ in a channel flow with an eddy promoter at $\lambda = 0.5$ and $D/d = 2$. Inserts in (a) show time-averaged Nusselt number, $\langle \overline{Nu} \rangle$, and in (b) time-averaged temperature, $\langle \overline{T} \rangle$, for each surface: —— upstream face, ---- top face, — — downstream face, ······ bottom face.

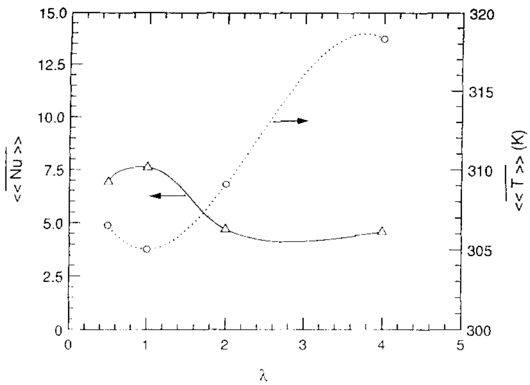

FIG. 12. Time- and total-surface-averaged values of Nusselt number and temperature as a function of λ with $Re = 592$ in a channel flow with $D/d = 2$. Data points plotted at $\lambda = 4$ correspond to the case of a single heated cylinder with $\lambda = \infty$.

function of the inter-cylinder spacing, λ. The figure indicates a peak in the Nusselt number for $\lambda = 1$ while temperature yields a corresponding minimum for that spacing. This finding shows that there exists an optimum location for the eddy promoter.

Figure 13 provides plots of time- and single surface-averaged temperatures for the four surfaces of the heated cylinder as a function of inter-cylinder spacing. The plots for the top and bottom surfaces show a decrease in temperature with decreasing λ. The upstream surface of the cylinder is insensitive to λ while the downstream surface shows an initial decrease in temperature with decreasing λ, until $\lambda = 1$ where the temperature now starts increasing with decreasing λ. Since it is the temperature of the downstream surface only which shows a minimum with λ, this surface is identified as the one responsible for

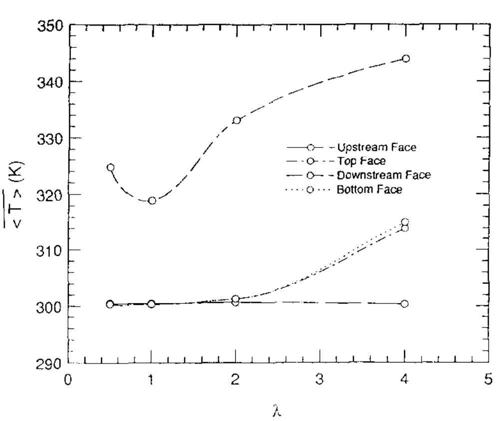

FIG. 13. Time- and single surface-averaged values of temperature for each of the four surfaces of the downstream cylinder of a pair with $D/d = 2$ and $Re = 592$ as a function λ. Data points plotted at $\lambda = 4$ correspond to the case of a single heated cylinder with $\lambda = \infty$.

the optimum inter-cylinder spacing discussed earlier.

Two questions remain to be answered: (1) Why is the heat transfer so large from the top and bottom surfaces of the heated cylinder when a smaller adiabatic cylinder is placed upstream of it? (2) Why does the temperature of the downstream surface of the heated cylinder show a minimum with λ? Flow visualization experiments performed with two square cylinders of diameter ratio $D/d = 2$ in the water channel provide answers. We first list the main observations of these experiments and subsequently interpret them from a heat transfer point of view.

(i) For inter-cylinder spacings which do not show eddy shedding from the upstream cylinder, the downstream cylinder sheds eddies at a frequency higher than the eddy shedding frequency for a single cylinder. It may be recalled that the numerical computations also showed the same phenomenon. However, from the experiments it is clear that the flow field between two cylinders is unsteady and the unsteadiness grows in amplitude as λ is increased. This unsteady flow region seems to trigger eddy shedding at a frequency larger than that corresponding to a single cylinder. (ii) At spacings for which the upstream cylinder begins to shed eddies, the downstream cylinder is induced to shed eddies at the same frequency. Whenever eddies from the upstream cylinder roll over the top or bottom surface of the downstream cylinder, they disturb the boundary layers on these surfaces. The result is an alternating transient thinning of each boundary layer which propagates as a wave along the length of each surface.

The increased eddy-shedding frequency of the downstream cylinder when the upstream cylinder is not shedding eddies provides a shorter time for the boundary layers to grow at the top and bottom surfaces of the downstream cylinder compared with the case of a single cylinder. This results in thinner boundary layers and provides a mechanism for enhancing heat transfer from the top and bottom surfaces, as observed in the numerical computations. Heat transfer from these surfaces does not diminish for larger inter-cylinder spacings because the boundary layers that are induced to grow on the top and bottom surfaces by the eddies from the upstream cylinder reattach before leaving the downstream cylinder. Thus, for the Re and λ values considered in the numerical computations, the average heat transfer from the top and bottom surfaces of the downstream heated cylinder is improved when compared to the case of a single heated cylinder and it is insensitive to λ. However, the time- and surface-averaged temperature of the downstream surface of the heated cylinder shows a minimum at $\lambda = 1$. This can be associated with the region of the vortex formation downstream of the heated cylinder. As the inter-cylinder spacing is reduced from $\lambda = \infty$ to 1, the region of vortex formation behind the heated cylinder moves closer to the downstream surface and thus enhances heat transfer. For $\lambda < 1$, the region of vortex formation moves away from the downstream surface and thereby decreases heat transfer.

6. CONCLUSIONS

A study of unsteady, two-dimensional flow past cylinders of square cross-section in tandem has been performed to further the fundamental understanding of the flow and heat transfer. The first configuration investigated is for equal-sized cylinders and provides qualitative insight into the basic structure of this type of bluff body flow as well as quantitative information for the dependence of the flow on cylinder spacing and Reynolds number. In this regard, phenomena not previously observed are reported. The effect of varying the relative cylinder dimensions was examined in a second problem using a small cylinder placed upstream of a large cylinder. In this case the investigation was extended to include heat transfer from the downstream cylinder. Flow visualization and numerical simulations were performed to provide complementary qualitative and quantitative descriptions of these flows. From these results the use of an eddy promoter is suggested for enhancing heat transfer from electronic components in ventilated enclosures.

The main results of the investigation are summarized as follows.

Problem A-A

Two distinct flow patterns exist above and below a critical cylinder spacing given by $\lambda_c = 168\ Re^{-2/3}$. Below this critical separation, the two counter-rotating eddies in the inter-cylinder recirculation region experience significant vertical oscillations, including the periodic ingestion of back-flowing fluid into the inter-cylinder gap. The oscillations and periodic backflows are attributed to the alternating transverse pressure gradient which is driven, primarily, by eddy-shedding in the wake of the downstream cylinder. At the critical separation, the commencement of eddy-shedding from the upstream cylinder is accompanied by discontinuous increases in the average drag coefficient of the downstream cylinder, and increases in the fluctuations of both the lift and drag coefficients of both cylinders about the mean. Instantaneous calculated velocity profiles also show the increased unsteadiness of the flow following the formation of a vortex street in the wake of the upstream cylinder. In a range of separations about the critical point, both of the above flow patterns are exhibited alternately, demonstrating the bistable nature of this transition.

Problem B-A

The above observations regarding the two distinct flow patterns also apply to this case. However, the frequency of eddy-shedding from the downstream cylinder is higher than for problem A-A. This increase is related to the reduction in the diameter of the upstream cylinder. Since for any flow there is only one Strouhal number associated with a given Reynolds number, for fixed velocity a reduction in cylinder diameter must be accompanied by a corresponding increase in its eddy-shedding frequency. The optimal spacing for the upstream cylinder was found to be smaller than the critical separation. The temperature of the upstream surface of the heated cylinder is relatively insensitive to the different inter-cylinder spacings investigated in this study. The temperatures of the top and bottom surfaces increase slightly with increasing inter-cylinder spacing. The temperature of the downstream surface shows a minimum at $\lambda = 1$ pointing to the existence of an optimal location for the eddy promoter.

Acknowledgements—This work was funded by a grant awarded by the IBM Corporation (Boca Raton/Austin) to advance Interactive Computational–Experimental Methodologies (ICEME) in thermofluids research of computer mechanics problems. The authors are very grateful both for this support and the interest shown by their colleagues at IBM in the work.

REFERENCES

1. A. Okajima, Strouhal numbers of rectangular cylinders, *J. Fluid Mech.* **123,** 379–398 (1982).
2. R. W. Davis and E. F. Moore, A numerical study of vortex shedding from rectangles, *J. Fluid Mech.* **116,** 475–506 (1982).
3. R. W. Davis, E. F. Moore and L. P. Purtell, Numerical–experimental study of confined flow around rectangles, *Phys. Fluids* **27,** 46–59 (1984).
4. T. Igarashi, Heat transfer from a square prism to an air stream, *Int. J. Heat Mass Transfer* **28,** 175–181 (1985).
5. T. Igarashi, Local heat transfer from a square prism to an air stream, *Int. J. Heat Mass Transfer* **29,** 777–784 (1986).
6. T. Igarashi, Fluid flow and heat transfer around rectangular cylinders (the case of a width/height ratio of a section of 0.33–1.5), *Int. J. Heat Mass Transfer* **30,** 893–901 (1987).
7. R. J. Goldstein, S. Y. Yoo and M. K. Chung, Convective mass transfer from a square cylinder and its base plate, *Int. J. Heat Fluid Flow* **33,** 9–18 (1990).
8. F. P. Incropera and D. P. De Witt, *Fundamentals of Heat and Mass Transfer*. Wiley, New York (1990).
9. M. M. Zdravkovich, Review of flow interference between two circular cylinders in various arrangements, *Trans. ASME* **99,** 618–633 (1977).
10. N. Shiraishi, M. Matsumoto and H. Shirato, On aerodynamic instabilities of tandem structures, *J. Wind Engng Ind. Aerodynamics* **23,** 437–447 (1986).
11. M. Hiwada, T. Taguchi, I. Mabuchi and M. Kumada, Fluid flow and heat transfer around two circular cylinders of different diameters in cross flow, *Bull. JSME* **22,** 715–723 (1979).
12. T. Ota, H. Nishiyama, J. Kominami and K. Sato, Heat transfer from two elliptic cylinders in tandem arrangement, *J. Heat Transfer* **108,** 525–531 (1986).
13. E. B. Treidler, An experimental and numerical investigation of flow past ribs in a channel, Ph.D. Thesis, University of California at Berkeley (1991).
14. C. A. Schuler, Investigation of the flow between rotating disks in an enclosure, Ph.D. Thesis, University of California at Berkeley (1990).
15. C. A. Schuler, E. B. Treidler and J. A. C. Humphrey, *CUTEFLOWS User's Guide*, Computer Mechanics Laboratory Report #CML91-001, University of California at Berkeley (1991).

16. J. A. C. Humphrey, C. A. Schuler and I. Iglesias, Analysis of viscous dissipation in disk storage systems and similar flow configurations, *Phys. Fluids A* **4**, 1415–1427 (1992).
17. A. J. Chorin and J. E. Marsden, *A Mathematical Introduction to Fluid Mechanics*. Springer, New York (1979).
18. M. P. Arnal, D. J. Goering and J. A. C. Humphrey, The influence of a solid boundary on vortex shedding from a bluff body, *J. Fluids Engng* **113**, 384–398 (1991).
19. K. Tatsutani, W. R. Usry and J. A. C. Humphrey, Numerical calculation of two-dimensional laminar flow and heat transfer for a backward facing step using CUTEFLOWS, Benchmark Problems for Heat Transfer Codes, 1992 ASME Winter Annual Meeting, Anaheim, California.
20. D. K. Gartling, A test problem for outflow boundary conditions—flow over a backward facing step, *Int. J. Numer. Meth. Fluids* **11**, 953–967 (1990).
21. K. Tatsutani and J. A. C. Humphrey, Experimental and numerical investigation of flow past square cylinders in tandem, Fluid Mechanics and Heat Transfer Laboratory Report #92-1, University of California at Berkeley (1992).
22. R. Devarakonda and J. A. C. Humphrey, Interactive computational–experimental methodologies in cooling of electronic components, Report #CML92-008, Computer Mechanics Laboratory, University of California at Berkeley (1992).